

Evidence of Sub-proton-scale Magnetic Holes in the Venusian Magnetosheath

Katherine Amanda Goodrich¹, John W. Bonnell², Shannon M. Curry³, Roberto Livi¹, Phyllis Whittlesey¹, Forrest Mozer¹, Marc Pulupa⁴, David M. Malaspina⁵, Stuart d Bale⁶, Trevor A Bowen⁷, Anthony William Case⁸, Thierry Dudok de Wit⁹, Keith Goetz¹⁰, Peter R Harvey¹, Jasper S. Halekas¹¹, Justin C. Kasper¹², Davin E. Larson¹, Robert John MacDowall¹³, Michael D McManus¹, and Michael Louis Stevens⁸

¹University of California, Berkeley

²University of California

³UC Berkeley

⁴Space Sciences Laboratory, University of California at Berkeley

⁵University of Colorado Boulder

⁶University of California, Berkeley

⁷Space Sciences Laboratory

⁸Harvard-Smithsonian Center for Astrophysics

⁹CNRS and University of Orléans

¹⁰University of Minnesota

¹¹University of Iowa

¹²University of Michigan-Ann Arbor

¹³NASA Goddard Space Flight Center

November 22, 2022

Abstract

Depressions in magnetic field strength, commonly referred to as magnetic holes, are observed ubiquitously in space plasmas. Sub-proton-scale magnetic holes with spatial scales smaller than or on the order of ρ_p , are likely supported by electron current vortices, rotating perpendicular to the ambient magnetic field. While there are numerous accounts of sub-proton-scale magnetic holes within the Earth's magnetosphere, there are no reported observations in other space plasma environments. We present the first evidence of sub-proton-scale magnetic holes in the Venusian magnetosheath. During Parker Solar Probe's first Venus Gravity Assist, the spacecraft crossed the planet's bow shock and subsequently observed the Venusian magnetosheath. The FIELDS instrument suite onboard the spacecraft achieved magnetic and electric field measurements of magnetic hole structures. The electric field associated with magnetic depressions are consistent with electron current vortices with amplitudes on the order of $1 \mu\text{A}/\text{m}^2$.

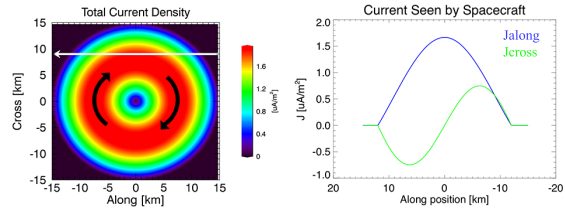
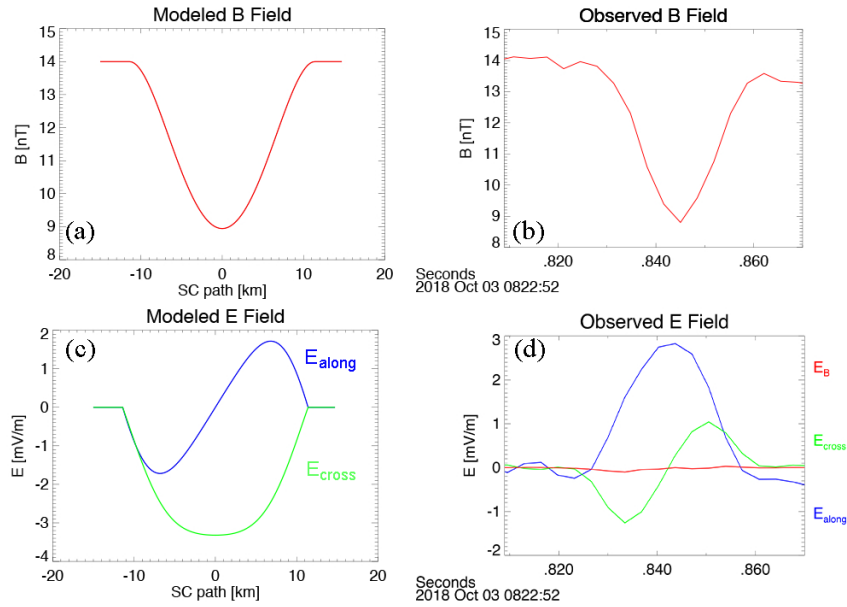
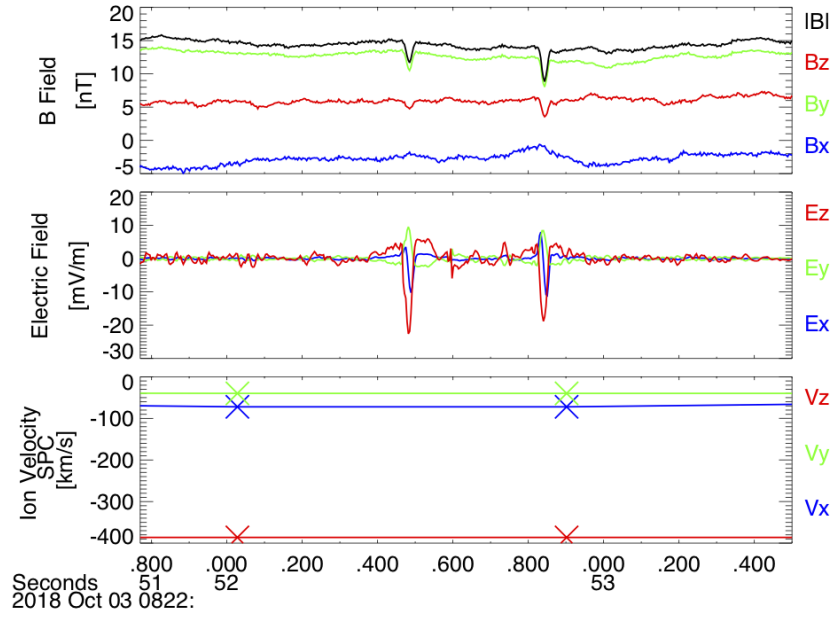
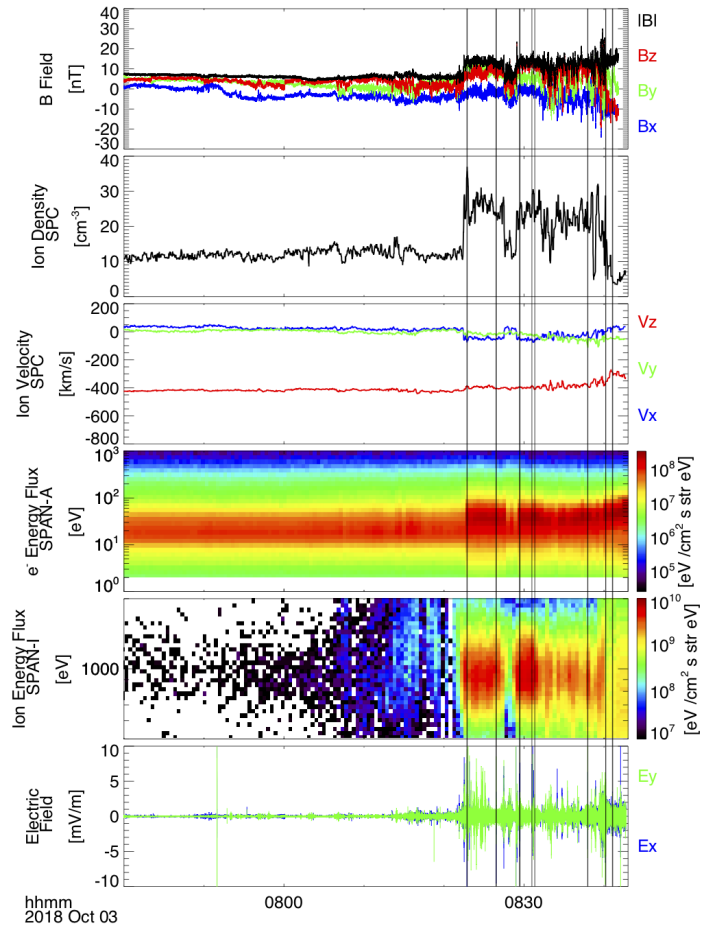


Figure 1. (Left) Two-dimensional view of total current density $|\mathbf{J}|$ of an electron vortex as a function of spatial scale (X and Y where the center is $X = Y = 0$), with a radius of 15 km. The current density profile is defined in Equation 1. The white arrow shows the spacecraft path across the structure. (Right) The current density theoretically seen in both the X and Y directions along the given spacecraft path.





Evidence of Sub-proton-scale Magnetic Holes in the Venusian Magnetosheath

Katherine A. Goodrich¹, John W. Bonnell¹, Shannon Curry¹, Roberto Livi¹,
Phyllis Whittlesey¹, Forrest Mozer^{1,2}, David Malaspina³, Jasper Halekas⁴,
Michael McManus^{1,2}, Stuart Bale^{1,2}, Trevor Bowen¹, Anthony Case⁵, Thierry
Dudok de Wit⁶, Keith Goetz⁷, Peter Harvey¹, Justin Kasper⁸, Davin Larson¹,
Robert MacDowall⁹, Marc Pulupa¹, Michael Stevens⁵

¹Space Sciences Laboratory, University of California, Berkeley, CA 94720-7450, USA

²Physics Department, University of California, Berkeley, CA 94720-7300, USA

³University of Colorado at Boulder, Boulder, CO, USA

⁴Department of Physics and Astronomy, University of Iowa, Iowa City, IA, USA

⁵Harvard-Smithsonian Center for Astrophysics, Cambridge, MA, USA

⁶University of Orléans, Orléans, France

⁷University of Minnesota, Minneapolis, MN, USA

⁸University of Michigan, Anna Arbor, MI, USA

⁹NASA, Goddard Space Flight Center, Greenbelt, MD, USA

Key Points:

- Magnetic depressions with spatial scales less than the local proton gyroradius are observed in the Venusian magnetosheath.
- Electric field associated with these depressions are consistent with electron current vortex structures.
- Similar structures have been observed in the terrestrial magnetosphere, suggesting they are part of a universal plasma process.

Abstract

Depressions in magnetic field strength, commonly referred to as magnetic holes, are observed ubiquitously in space plasmas. Sub-proton-scale magnetic holes with spatial scales smaller than or on the order of ρ_p , are likely supported by electron current vortices, rotating perpendicular to the ambient magnetic field. While there are numerous accounts of sub-proton-scale magnetic holes within the Earth's magnetosphere, there are no reported observations in other space plasma environments. We present the first evidence of sub-proton-scale magnetic holes in the Venusian magnetosheath. During Parker Solar Probe's first Venus Gravity Assist, the spacecraft crossed the planet's bow shock and subsequently observed the Venusian magnetosheath. The FIELDS instrument suite on-board the spacecraft achieved magnetic and electric field measurements of magnetic hole structures. The electric field associated with magnetic depressions are consistent with electron current vortices with amplitudes on the order of $1 \mu\text{A}/\text{m}^2$.

Plain Language Summary

The Sun is constantly ejecting an ionized gas, or plasma. This plasma from this Sun is called the solar wind and usually consists of an equal number of negatively charged electrons and their larger positively charged counterparts, protons. These particles travel together from the Sun, cancelling out each other's charge. When the plasma encounters obstacles, however, like the Earth or Venus, the plasma becomes disturbed. This can cause the electrons can separate from the protons and form unbalanced structures. One interesting structure that has recently been discovered at Earth are electron vortices. These vortices can create their own magnetic and electric fields and slightly alter the plasma around them. We have seen electron vortices where the solar wind meets the Earth, but are not sure how they are created or how strongly they affect the plasma around them. We report, for the first time, evidence of electron vortices where the solar wind encounters Venus. These new findings show the process that creates electron vortices takes place at both Earth and Venus, strongly implying a universal process in space.

1 Introduction

Sub-proton-scale magnetic holes are depressions in total magnetic field (\mathbf{B}) strength with spatial scales less than, or on the order of, a proton gyroradius (ρ_p). Depressions in $|\mathbf{B}|$ that are spatially larger than ρ_p can usually be attributed to the magnetic mir-

55 ror instability (Southwood & Kivelson, 1993), so much so they are commonly referred
56 to as mirror mode waves. Mirror mode waves have been observed frequently in multi-
57 ple space plasma environments such as the solar wind (Wintertialter et al., 1994; Rus-
58 sell et al., 2008) and terrestrial magnetosheath (Johnson & Cheng, 1997; Soucek et al.,
59 2008). They are generally known to be generated via a plasma temperature anisotropy
60 (Califano et al., 2008; Kuznetsov et al., 2008).

61 Sub-proton-scale magnetic holes are measured to be less than or on the order of
62 the local proton gyroradius, and therefore cannot be explained by the mirror instabil-
63 ity. Also, unlike mirror-wave modes, sub-proton-scale magnetic holes are observed with
64 features consistent with current layers carried by electrons (Gershman et al., 2016; Goodrich,
65 Ergun, & Stawarz, 2016). While the structure may extend longer than a ρ_p (Goodrich,
66 Ergun, & Stawarz, 2016)), the current layers associated with sub-proton-scale magnetic
67 holes have spatial scales smaller than ρ_p . Sub-proton-scale magnetic holes have been ob-
68 served within the Earth's magnetosphere during times of magnetic field fluctuations, par-
69 ticularly in the magnetosheath (Huang et al., 2017; Liu et al., 2019; Yao et al., 2017) and
70 near-Earth plasmashet (Ge et al., 2011; Sun et al., 2012; Tenerani et al., 2012, 2013;
71 Sundberg et al., 2015; Gershman et al., 2016). Currents carried by such electron vortices
72 have been observed both through high resolution particle measurements from the Mag-
73 netospheric Multiscale (MMS) mission (Gershman et al., 2016) as well as electric field
74 measurements (Goodrich, Ergun, Wilder, et al., 2016a) from both MMS and THEMIS
75 (Goodrich, Ergun, & Stawarz, 2016).

76 Sub-proton-scale magnetic holes are often thought to arise through a the nonlinear
77 evolution the mirror instability and the tearing instability (Ahmadi et al., 2017; Balikhin
78 et al., 2010, 2012). This has not been observationally confirmed. Additionally, the sim-
79 ulations performed by Haynes et al. (2015) and Roytershteyn et al. (2015) suggest sub-
80 proton-scale magnetic holes arise as a coherent structure in plasma turbulence. The spa-
81 tial size of sub-proton-scale magnetic holes ($< \rho_p$), however, excludes them from the mir-
82 ror instability. The tearing instability is also insufficient to explain these structures as
83 the required shear in perpendicular magnetic field components has not been observed.

84 While observations of sub-proton-scale magnetic holes have become increasingly
85 frequent in recent years, their role and importance to space plasma physics is not well
86 known. Confirmed reports of sub-proton-scale magnetic holes in both the terrestrial mag-

netosheath and plasmashet suggest they may be a product of a universal process. However, there are currently no observations of such signatures that extend beyond the terrestrial magnetosphere. This is likely due to the fact that structures with this spatial scale is difficult to observe given the time resolution limitations on particle instruments available on previous missions to Venus, Mercury, and Mars. Additionally, the majority of these missions do not possess a full range of electric field observations, which can also be used to observe electron currents.

We report, for the first time, evidence of structures bearing significant similarities to sub-proton-scale magnetic holes in the Venusian magnetosheath. These structures were observed by the Parker Solar Probe (PSP) spacecraft during its initial Venus Gravity Assist (VGA1). Significant depressions in magnetic field strength (up to 30% of the original $|\mathbf{B}|$ value) were observed at length scales less than the local thermal proton gyro-radius throughout the Venusian magnetosheath. These magnetic depressions have corresponding unipolar and bipolar electric field signals that are consistent with the presence of electron vortices.

In this paper, we review the observations from VGA1, and the magnetic hole structures found within. We then compare these observations with a simple model of an electron vortex. This comparison shows the observed signatures are largely consistent with electron vortices. These observations bear strong similarities to sub-proton-scale magnetic holes observed in the terrestrial magnetosphere. This report suggests these structures are indicative of a universal, or pervasive, process in magnetospheric plasmas.

2 Data and Instruments

The measurements examined in this study are taken from the Parker Solar Probe mission (Fox et al., 2016). Its purpose is to measure the young solar wind by obtaining measurements as close as nine solar radii from the surface of the Sun. In order for the spacecraft to reach this destination, it must encounter Venus seven times for gravitational assistance. Here we examine fields and particle measurements taken during the first Venus gravity assist, heretofore referred to as VGA1, on October 3rd, 2018 between 07:00 and 08:50 UTC.

Observations of electric field and magnetic field were obtained via the FIELDS instrument suite (Bale et al., 2016; Malaspina et al., 2016). This suite measures magnetic

118 field from two fluxgate magnetometers (FGM) as well as a search coil magnetometer (SCM),
 119 all of which are mounted on the magnetometer boom directly behind the heat shield. Four
 120 2 m antennas, which measure electric potentials V_1 , V_2 , V_3 , and V_4 , are positioned in the
 121 plane of the heat shield, perpendicular to the sun-spacecraft direction. The fifth poten-
 122 tial, V_5 , is measured by a 21 cm antenna, also mounted on the magnetometer boom. The
 123 electric field in the plane of the heat shield is derived from the differential voltage mea-
 124 surements ($V_1 - V_2$ and $V_3 - V_4$) calculated on the spacecraft.

125 The electric fields were calibrated by least squares fitting twelve second averages
 126 of E_X versus $-(v_i \times \mathbf{B})_X$ and E_Y versus $-(v_i \times \mathbf{B})_Y$, where v_i is the proton velocity
 127 from SPC. The four least squares coefficients were two dc offsets resulting from electronic
 128 offsets, the effective antenna length, and an angular rotation of the fields in the X-Y plane.
 129 This rotation was found necessary and may have resulted because the electric field an-
 130 tenna was comparable in size to the spacecraft and the Debye length, as described fur-
 131 ther in **Mozer et al., (2020, submitted)**.

132 All particle measurements used in this analysis were provided by the Solar Wind
 133 Electrons Alphas and Protons (SWEAP) instrument suite (Kasper et al., 2016). Elec-
 134 tron moments and distributions were measured by the SPAN-electron instrument (Halekas
 135 et al., 2020; Whittlesey et al., 2020). Ion moments and distributions were measured by
 136 the Solar Probe Cup (SPC) (Case et al., 2020) and SPAN-ion (Kasper et al., 2016) in-
 137 struments. SPC has a 40° half-angle field of view, with its center pointed directly sun-
 138 ward. SPAN-ion has a $120^\circ \times 247.5^\circ$ view of the sky perpendicular to the sunward di-
 139 rection. The combination of SPC and SPAN-ion provides a nearly full view of the sky.
 140 During VGA1, SPC had a 1.3 second temporal resolution. SPAN-electron and SPAN-
 141 ion had a temporal cadence of ~ 28 seconds.

142 A detailed description of the first Parker Solar Probe Venus Gravity Assist as well
 143 as its implications are reported by **Curry et al., [2020] (this issue)**. Figure 1 shows
 144 an overview of VGA1, which displays magnetic field, proton density (n_p), proton veloc-
 145 ity (\mathbf{V}_p), electron energy flux, ion energy flux from SPAN-ion, and high pass filtered elec-
 146 tric field (all signal below 1 Hz removed), in descending order. All vectors are shown in
 147 the spacecraft frame, where Z is pointed sunward and X is pointed along the spacecraft
 148 trajectory in the plane of the heat shield. It is of note that these measurements are the
 149 first ever current-biased DC electric field measurements at Venus.

150 All proton measurements examined are taken from SPC unless otherwise stated.
 151 For all \mathbf{V}_p , n_p , and temperature (T_p , not displayed) moments, the times at which $n_p =$
 152 0 were removed. All data were subsequently median smoothed over eleven consecutive
 153 point intervals. The focus of this study are structures with spatial scales less than ρ_p ,
 154 which are observed over tens of milliseconds. This time frame is well below the time res-
 155 olution of all available particle instruments and therefore this treatment of the particle
 156 data is appropriate to provide overall context of the plasma environment during VGA1.

157 The PSP spacecraft made its approach traveling in the sunward direction and en-
 158 countered the Venusian environment on its dawnward-flank side. Between 7:00 and 8:00
 159 UTC, the spacecraft detected solar wind plasma. This is evident from steady proton den-
 160 sity and antisunward velocity at 10 cm^{-3} and 450 km/s respectively. There are no co-
 161 herent features observed by SPAN-ion and the magnetic field remains at a constant am-
 162 plitude of $\sim 5 \text{ nT}$. The spacecraft subsequently (between 8:00 and 8:22 UTC) observes
 163 magnetic fluctuations and broad energy signals in ion energy flux from SPAN-ion. This
 164 indicates ion flows outside of the SPC field of view, which is consistent with the pres-
 165 ence of reflected ions from the Venusian bow shock.

166 PSP likely crossed the Venusian bow shock and entered the magnetosheath for the
 167 first time at $\sim 08:22:20 \text{ UTC}$. This is indicated by the abrupt increase in $|\mathbf{B}|$ and n_p , as
 168 well as a deviation in proton velocity. The spacecraft subsequently crossed the bow shock
 169 approximately five times before it approached the magnetic pile-up region at 8:50 UTC.
 170 At this time all instruments were powered off due to a solar limb sensor anomaly, and
 171 no further data were collected during the encounter.

172 The vertical lines in Figure 1 highlight times in which sub-proton-scale magnetic
 173 hole candidates were observed. Eleven candidates were identified after the initial bow
 174 shock crossing in the Venusian magnetosheath. These structures were identified by a dis-
 175 tinct decrease in $|\mathbf{B}|$, as well as corresponding \mathbf{E} field signatures, with observation times
 176 over tens of milliseconds. The candidates identified showed no overall change in the av-
 177 erage (over one second) magnetic field. They were also observed alongside electric field
 178 signatures that will be discussed in depth in the following sections of this paper. All can-
 179 didates were found within the Venusian magnetosheath. No magnetic holes were observed
 180 in the solar wind or foreshock regions prior to observing the initial shock crossing, sug-

181 gesting they are generated through a process that takes place within the Venusan mag-
 182 netosheath.

183 3 Magnetic Hole Observations

184 Figure 2 shows an example of two magnetic hole candidates. It shows a 1.5 second
 185 zoomed in view of the magnetic field, electric field and proton velocity at $\sim 8:22:52$ UTC,
 186 ~ 30 seconds after the spacecraft's initial encounter with the Venusan bow shock. All
 187 vectors are shown in the spacecraft frame. E_x and E_y are directly measured by the four
 188 voltage probes in the plane aligned with the heat shield. E_z is calculated under the as-
 189 sumption that $\mathbf{E} \cdot \mathbf{B} = 0$. This assumption is appropriate as all observed electric field
 190 associated with sub-proton-scale magnetic holes have been primarily perpendicular to
 191 the magnetic field (Goodrich, Ergun, Wilder, et al., 2016b, 2016a).

192 The observed $\Delta|\mathbf{B}|/|\mathbf{B}|$ for each event is $\sim 35\%$ ($\sim 5/14$ nT) and the magnetic field
 193 direction shows little deviation ($\sim 2^\circ$) from the surrounding magnetic field. Both events
 194 are observed over 50 ms. The spatial length of the structure can be found under the as-
 195 sumption that it is stationary in the plasma (i.e. solar wind proton) frame. Sub-proton-
 196 scale magnetic holes have been shown to travel with the plasma by Liu et al. (2019). The
 197 spatial length of the magnetic holes are estimated to be 20 km, as the protons are mea-
 198 sured to travel ~ 400 km/s anti-sunward. This scale falls within the sub-proton-scale as
 199 the estimated proton gyroradius in this region is 40 km ($\sqrt{m_p T_p / B^2}$, derived via obser-
 200 vations from the flux gate magnetometer and proton temperature moments from SPC).
 201 These characteristics are all consistent with prior observations of sub-proton-scale mag-
 202 netic holes in the terrestrial context.

203 Electric field signals are seen in conjunction with the observed magnetic field de-
 204 pressions. A unipolar pulse reaching ~ 10 mV/m and ~ 20 mV/m is seen in the Y and
 205 Z directions respectively. A bipolar signal with an amplitude of ~ 10 mV/m is seen in
 206 the X direction. These signatures are qualitatively consistent with sub-proton-scale mag-
 207 netic holes observed in the Earth's magnetosphere. These signals bear similarities to elec-
 208 trostatic solitary waves like electron phase-space holes (EHs) and ion phase-space holes
 209 (IHs) (Ergun et al., 1998). It is, however, very unlikely that these signatures can be iden-
 210 tified as either. These structures are expected to travel at the electron and proton ther-
 211 mal speeds (v_{Te} , v_{Tp}) respectively (Ergun et al., 1998) and have spatial scales on the or-

212 der of 10s (EHs) to 100s (IHs) of Debye lengths (λ_D). Electron temperatures in the mag-
 213 netosheath are measured to be on the order of 40 eV (from the method described in Halekas
 214 et al. (2020)), which corresponds to a v_{Te} of 3750 km/s. This yields a scale size of 188
 215 km for a structure observed over 50 ms in the Venusian magnetosheath. This is 18800
 216 times greater than λ_D , estimated to be 10 m.

217 The electric fields in Figure 2 may be more consistent with IHs, which have an es-
 218 timated to have a scale size of 3.25 km (over 50 ms, given a proton temperature of 22
 219 eV measured from SPC). It is possible for IHs to produce a magnetic signal under a Lorentz
 220 transformation from the IH frame to the spacecraft frame. However, under the Lorentz
 221 transformation, an IH traveling at v_{Tp} produces a change in $|\mathbf{B}|$ of 0.2 fT. In order to
 222 produce the observed decrease in $|\mathbf{B}|$ (~ 5 nT), an IH with an E field amplitude of 20 mV/m
 223 must have a relative velocity of 2×10^6 km/s, 2/3 the speed of light.

224 Given the above parameters, it is far more likely that the observed magnetic de-
 225 pressions are caused by diamagnetic electron currents, rather than electrostatic solitary
 226 waves. It is of note that there are many observed solitary waves in the Venusian mag-
 227 netosheath with no magnetic field depletions. These waves may correspond to sub-proton-
 228 scale magnetic holes under different conditions. They may also correspond to electro-
 229 static solitary waves, dust impacts or other unexplored phenomena. This paper, how-
 230 ever, focuses on the electric field signatures with observable magnetic field depletions.

231 4 Model

232 In order to interpret these observations, we propose of a model of a sub-proton-scale
 233 magnetic hole and compare it's magnetic and electric field structures to the observed fea-
 234 tures. We construct a cylindrically symmetric current vortex. The current in this model
 235 is carried solely by electrons and is stationary in the plasma frame. The current J_ϕ is
 236 defined as

$$J_\phi = \begin{cases} J_0 \sin\left(\frac{\pi r}{2R}\right) & \text{if } r \leq R \\ 0 & \text{if } r > R \end{cases} \quad (1)$$

237 where r is the radial distance from the center of the magnetic hole and R is the estimated
 238 radius of the magnetic hole structure. J_0 is the maximum current density within the struc-
 239 ture. We then simulated a spacecraft crossing this structure in various trajectories.

240 Multiple trajectories and values of J_0 and R were tested with this model. All tra-
 241 jectories were parallel to the along-track direction, while the offset distance from the cen-
 242 ter of the structure in the cross-track direction varied. The trajectory is assumed to be
 243 perpendicular to the axis of symmetry of the vortex. The magnetic and electric field in-
 244 duced by the vortex were then calculated based on the defined spacecraft trajectory.

The induced magnetic field from this current is derived using Amperes law,

$$\Delta \mathbf{B}_Z(r_{SC}) = \frac{\mu_0}{R} \int_{r_{SC}}^R J_\phi(r) r dr. \quad (2)$$

The resulting magnetic field then becomes $\mathbf{B}_Z(r_{SC}) = \mathbf{B}_Z(R) - \Delta \mathbf{B}_Z(r_{SC})$, where r_{SC} is the radial position of the simulated spacecraft. The electric field was derived via the Lorentz equation (Stix, 1992),

$$\mathbf{E}_R(x_{SC}, y_{SC}) = -\mathbf{v}_e(x_{SC}, y_{SC}) \times \mathbf{B}_Z(r_{SC}). \quad (3)$$

245 The electron velocity as a function of spacecraft position ($\mathbf{v}_e(x_{SC}, y_{SC})$) was determined
 246 by $\mathbf{v}_e = -J_\phi(r_{SC})/qn_e$. \mathbf{v}_e is estimated to be on the order of 2000 km/s, calculated
 247 from $\mathbf{E} \times \mathbf{B}$ measurements from PSP. The density of the current layer, n_e , can there-
 248 fore be estimated by $J_0/q\mathbf{E}_R \times \mathbf{B}_Z$. This calculation is expected to be less than the mea-
 249 sured proton density n_p measured by SPC ($\sim 30 \text{ cm}^{-3}$).

250 The parameters of the model, particularly the radius of the structure (R), current
 251 density amplitude (J_0), and offset of the trajectory from the center of the vortex were
 252 all varied to best replicate the characteristics of the second magnetic hole candidate in
 253 Figure 2. Under the assumption that the structure is stationary in the plasma frame R
 254 must be on the order of $V_{SPC}\Delta t/2$ (10 km). J_0 was chosen such that the induced mag-
 255 netic field produced the same $\Delta|\mathbf{B}|$ observed by PSP ($\sim 5 \text{ nT}$).

256 We found the following values to be consistent with the chosen example:

- 257 • $R = 15 \text{ km}$
- 258 • $J_0 = 1.75 \mu\text{A/m}^2$
- 259 • Offset = 9 km
- 260 • $n_e = 5.5 \text{ cm}^{-3}$

261 Figure 3 shows a direct comparison between the observed magnetic and electric field of
 262 the sub-proton-scale magnetic hole (b and d) and those derived by the model (a and c)
 263 with the listed parameters. The observed \mathbf{E}_R and \mathbf{B}_Z vectors in this figure were rotated

264 into the plasma frame where the red vector ("B") is aligned with the magnetic field. The
 265 blue vector ("along") signifies the proton flow direction (perpendicular to the magnetic
 266 field), this is analogous to the "along-track" direction. The green vector ("cross") is aligned
 267 in the "cross-track" direction.

268 The modeled magnetic field decreases by 5.3 nT, matching the observed $\Delta|\mathbf{B}|$ ob-
 269 served by PSP (5.2 nT). This overall decrease is observed over 23 km in the model, which
 270 is further consistent with the observation time of the structure (~ 20 km). The modeled
 271 electric fields also bear certain similarities to observations. Firstly, the amplitudes of the
 272 modeled electric field (~ 9.75 and 16 mV/m for along and cross track respectively) are
 273 consistent with those observed (~ 25 and ~ 8 mV/m). The ratio of these amplitudes is
 274 approximately $1/2$ in the model and $1/3$ in observations, suggesting the modeled tra-
 275 jectory offset is consistent with the trajectory of the PSP spacecraft.

276 The electric fields derived from the model, however, deviate in direction from the
 277 observations by $\sim 90^\circ$. It is unclear, at this time, what the reason is for this deviation.
 278 One likely source of error may be contamination from a plasma wake from the spacecraft.
 279 Another source of error may be that the full plasma flow in the Venusian magnetosheath
 280 may lie partially outside of the field of view of the SPC and SPAN-ion instruments. All
 281 of the above may influence our analysis.

282 5 Discussion

283 In the previous section, we constructed an electron current vortex model with the
 284 intention of recreating observations from the Parker Solar Probe in the Venusian mag-
 285 netosheath. This model is consistent with most of the characteristics of observed sub-
 286 proton-scale magnetic holes. The current vortex model matches the estimated size of the
 287 observed magnetic hole. The induced a magnetic field from the model is also consistent
 288 (within 2%) with the $\Delta|\mathbf{B}|$ observed by PSP. The model also produced electric fields with
 289 amplitudes similar to those observed (on the order of 10 mV/m, within 35%). The elec-
 290 tric fields induced in the model, however, does not match the orientation of the fields seen
 291 in the observations. In fact, the observed electric fields deviate $\sim 90^\circ$ from the model.

292 The electric fields from all other magnetic hole candidates were also rotated in the
 293 plasma frame. All candidates deviated close to 90° in the azimuthal direction from the

294 model, in addition to the candidate in Figure 3. This suggests the deviation is related
 295 to a systematic or instrumental issue, rather than an issue from the plasma itself.

296 Contamination from a plasma wake is likely to contribute the most significant er-
 297 ror in this case. The electric field instrument consists of four single voltage probes, V1,
 298 V2, V3 and V4. Two-dimensional electric field are constructed by taking the potential
 299 difference between two pairs V1 - V2 (dV12) and V3 - V4 (dV34). These probe pairs are
 300 nearly, but not fully, orthogonal. V3 is oriented 40° from the anti-ram direction of the
 301 spacecraft while V2 deviate 55° . As such, V3 lies more parallel to the heat shield in the
 302 anti-ram direction and thus more likely to be contaminated by the potentials due to the
 303 spacecraft's plasma wake.

304 During VGA1, V3 measured an electric potential that differed significantly from
 305 V1, V2, and V4. In the Venusian magnetosheath, the average electric potential between
 306 V1 and V2 differs up to 50 mV. The potential difference between V3 and V4 is approx-
 307 imately 130 mV, almost 3 times greater. The potential difference between V3 and V4
 308 is even higher in the solar wind observed prior to the initial shock crossing, ~ 240 mV
 309 (6 times greater than V1 - V2).

310 Such a large deviation in potential suggests that V3 experiences plasma and po-
 311 tential conditions that are significantly different from those seen on V1, V2 and V4. The
 312 fact that this deviation changes when crossing from the solar wind into the Venusian mag-
 313 netosheath suggests the effect is dependent on overall plasma conditions. Both of these
 314 points are consistent with the effects of a plasma wake.

315 At this time, it is unclear the what the exact contribution of this possible wake ef-
 316 fect is on electric potential and field measurements. Contamination of V3 can indeed pro-
 317 duce an error in V3 - V4, which can cascade into the derivation of both E_X and E_Y in
 318 spacecraft coordinates. Moreover, the computation of the third component, E_Z , is re-
 319 liant on E_X and E_Y via $\mathbf{E} \cdot \mathbf{B} = 0$. As a result, the error produced by this wake effect
 320 will strongly affect all three components of the electric field.

321 Additionally, the electric fields were rotated according to proton velocity measure-
 322 ments from SPC. Velocity moments from SPAN-ion were also examined, but also resulted
 323 in a 90° deviation from the model. However, it is possible that, within the Venusian mag-
 324 netosheath, the full plasma distribution was not measured. SPC is directed sunward and

325 requires the core of the plasma distribution to be within 30° of its field-of-view (FOV)
326 before the measurement degrades. Due to the orientation of the spacecraft, SPAN-ion
327 was not pointed in the ram flow direction for the VGA1. The consequence is that only
328 a partial distribution function of ions was measured, which affects and partially skews
329 the derived plasma parameters. Velocities moments will inherently contain this offset if
330 the core of the distribution is not in the FOV. Three-dimensional bi-maxwellians fits to
331 the raw data can partially account for a part of this offset (Livi, private communication).

332 While the orientation of the observed electric field differs from those induced from
333 the current vortex model by 90° , the spatial size, \mathbf{E} field amplitude, and induced $\Delta|\mathbf{B}|$
334 of the model are remarkably consistent with all observations. While the orientation of
335 the electric field highlights specialized analysis is necessary during VGA1, there is suf-
336 ficient evidence to support that these magnetic hole signatures are consistent with elec-
337 tron current vortices.

338 According to our analysis, a current vortex with an amplitude of 1.75 A/m^2 is re-
339 quired to induce the observed decrease in $|\mathbf{B}|$ shown in Figures 2 and 3. The electric fields
340 seen with these $|\mathbf{B}|$ decreases suggest the current corresponds to electrons traveling at
341 speeds on the order of 1000 km/s , up to 5 times faster than the observed proton veloc-
342 ity moments. Moreover, at least eleven sub-proton-scale magnetic holes were identified
343 throughout PSP's encounter with Venus. This suggests these structures are a common
344 structure within the Venusian magnetosheath.

345 As stated previously, sub-proton-scale magnetic holes have arisen in multiple plasma
346 turbulence simulations (Haynes et al., 2015; Roytershteyn et al., 2015). They have been
347 suggested as a coherent structure that can arise naturally through turbulence. Obser-
348 vations in the terrestrial magnetosheath have also shown that sub-proton-scale magnetic
349 holes can be seen with electron trapping (Huang et al., 2017) and electron heating per-
350 pendicular to the magnetic field (Liu et al., 2019). It is therefore possible that these struc-
351 tures may play a role or be a signature of turbulent dissipation. It is also possible they
352 have evolved from other mechanisms (e.g. the mirror or tearing instability). What is clear,
353 however, is the process that generates sub-proton-scale magnetic holes are present at both
354 Earth and Venus.

6 Conclusion

On October 3rd, 2018, the Parker Solar Probe spacecraft encountered the Venusian magnetosheath as part of a gravity assist maneuver. During this encounter, localized depressions in magnetic field strength were observed with spatial scales less than the local thermal proton gyroradius, consistent with characteristics of sub-proton-scale magnetic holes. Eleven sub-proton-scale magnetic hole candidates were identified within the Venusian magnetosheath. No candidates were found in the solar wind during prior to the initial shock crossing.

Sub-proton-scale magnetic holes have been observed in many regions of the terrestrial magnetosphere with diverse plasma conditions. It is now clear, by additional reports of their presence at Venus, that they are indicative of a universal plasma process. Additionally, these observations, as well as the modeled comparison, suggest that the Venusian magnetosheath is host to widespread, large-amplitude, small-scale, electron current structures. It is unclear how such structures manifest or how they affect their plasma environment. Their importance to Venusian microphysics is consequently unclear. Understanding them, however, can lead to unprecedented insights to the microphysical processes that occur within the Venusian magnetosphere.

The Parker Solar Probe mission will engage in a total of seven flybys of Venus. These flybys cover multiple regions of the Venusian space plasma environment, including the bow shock, foreshock and magnetotail. With the advanced capabilities available on Parker Solar Probe, we stand to gain a better understanding of the microphysics that take place at Venus than we ever had and place those processes within the broader context of planetary electrodynamics across the inner solar system.

Acknowledgments

This work was made possible by the Parker Solar Probe mission. The FIELDS experiment on the Parker Solar Probe spacecraft was designed and developed under NASA contract NNN06AA01C. All data are available at <http://fields.ssl.berkeley.edu/>.

References

Ahmadi, N., Germaschewski, K., & Raeder, J. (2017). Simulation of magnetic holes formation in the magnetosheath. *Physics of Plasmas*, *24*(12). Retrieved from

- 385 <http://dx.doi.org/10.1063/1.5003017> doi: 10.1063/1.5003017
- 386 Bale, S. D., Goetz, K., Harvey, P. R., Turin, P., Bonnell, J. W., de Wit, T., ...
 387 Wygant, J. R. (2016, 12). The FIELDS Instrument Suite for Solar Probe Plus.
 388 *Space Science Reviews*, 204(1), 49–82. Retrieved from [https://doi.org/](https://doi.org/10.1007/s11214-016-0244-5)
 389 [10.1007/s11214-016-0244-5](https://doi.org/10.1007/s11214-016-0244-5) doi: 10.1007/s11214-016-0244-5
- 390 Balikhin, M. A., Pokhotelov, O. A., Walker, S. N., Boynton, R. J., & Beloff, N.
 391 (2010). Mirror mode peaks: THEMIS observations versus theories. *Geophysical*
 392 *Research Letters*, 37(5), n/a-n/a. doi: 10.1029/2009gl042090
- 393 Balikhin, M. A., Sibeck, D. G., Runov, A., & Walker, S. N. (2012). Mag-
 394 netic holes in the vicinity of dipolarization fronts: Mirror or tearing struc-
 395 tures? *Journal of Geophysical Research: Space Physics*, 117(8), 1–14. doi:
 396 [10.1029/2012JA017552](https://doi.org/10.1029/2012JA017552)
- 397 Califano, F., Hellinger, P., Kuznetsov, E., Passot, T., Sulem, P. L., & TráVn\`iĉEk,
 398 P. M. (2008, 8). Nonlinear mirror mode dynamics: Simulations and mod-
 399 eling. *Journal of Geophysical Research (Space Physics)*, 113, A08219. doi:
 400 [10.1029/2007JA012898](https://doi.org/10.1029/2007JA012898)
- 401 Case, A. W., Kasper, J. C., Stevens, M. L., Korreck, K. E., Paulson, K., Daigneau,
 402 P., ... Martinović, M. M. (2020, 2). The Solar Probe Cup on the Parker
 403 Solar Probe. *The Astrophysical Journal Supplement Series*, 246(2), 43.
 404 Retrieved from <https://doi.org/10.3847/1538-4365/2020ab5a7b> doi:
 405 [10.3847/1538-4365/ab5a7b](https://doi.org/10.3847/1538-4365/ab5a7b)
- 406 Ergun, R. E., Carlson, C. W., Mc Fadden, J. P., Mozer, F. S., Muschietti, L., Roth,
 407 I., & Strangeway, R. J. (1998, 7). Debye-scale plasma structures associated
 408 with magnetic-field-aligned electric fields. *Physical Review Letters*, 81(4),
 409 826–829. doi: 10.1103/PhysRevLett.81.826
- 410 Fox, N. J., Velli, M. C., Bale, S. D., Decker, R., Driesman, A., Howard, R. A., ...
 411 Szabo, A. (2016, 12). The Solar Probe Plus Mission: Humanity’s First Visit
 412 to Our Star. *Space Science Reviews*, 204(1), 7–48. Retrieved from [https://](https://doi.org/10.1007/s11214-015-0211-6)
 413 doi.org/10.1007/s11214-015-0211-6 doi: 10.1007/s11214-015-0211-6
- 414 Ge, Y. S., McFadden, J. P., Raeder, J., Angelopoulos, V., Larson, D., & Constan-
 415 tinescu, O. D. (2011, 1). Case studies of mirror-mode structures observed
 416 by THEMIS in the near-Earth tail during substorms. *Journal of Geophysical*
 417 *Research (Space Physics)*, 116, A01209. doi: 10.1029/2010JA015546

- 418 Gershman, D. J., Dorelli, J. C., Viñas, A. F., Avannov, L. A., Gliese, U., Barrie,
 419 A. C., . . . Burch, J. L. (2016). Electron dynamics in a subproton-gyroscale
 420 magnetic hole. *Geophysical Research Letters*. doi: 10.1002/2016GL068545
- 421 Goodrich, K. A., Ergun, R. E., & Stawarz, J. E. (2016). Electric fields associated
 422 with small-scale magnetic holes in the plasma sheet: Evidence for electron
 423 currents. *Geophysical Research Letters*. doi: 10.1002/2016GL069601
- 424 Goodrich, K. A., Ergun, R. E., Wilder, F. D., Burch, J., Torbert, R., Khotyaintsev,
 425 Y., . . . Malaspina, D. M. (2016a). MMS Multipoint electric field observa-
 426 tions of small-scale magnetic holes. *Geophysical Research Letters*, *43*(12),
 427 5953–5959. doi: 10.1002/2016GL069157
- 428 Goodrich, K. A., Ergun, R. E., Wilder, F. D., Burch, J., Torbert, R., Khotyaintsev,
 429 Y., . . . Malaspina, D. M. (2016b). MMS Multipoint electric field obser-
 430 vations of small-scale magnetic holes. *Geophysical Research Letters*. doi:
 431 10.1002/2016GL069157
- 432 Halekas, J. S., Whittlesey, P., Larson, D. E., McGinnis, D., Maksimovic, M.,
 433 Berthomier, M., . . . Harvey, P. R. (2020). Electrons in the Young Solar
 434 Wind: First Results from the Parker Solar Probe . *The Astrophysical Journal*
 435 *Supplement Series*, *246*(2), 22. Retrieved from [http://dx.doi.org/10.3847/](http://dx.doi.org/10.3847/1538-4365/ab4cec)
 436 [1538-4365/ab4cec](http://dx.doi.org/10.3847/1538-4365/ab4cec) doi: 10.3847/1538-4365/ab4cec
- 437 Haynes, C. T., Burgess, D., Camporeale, E., & Sundberg, T. (2015, 1). Electron
 438 vortex magnetic holes: A nonlinear coherent plasma structure. *Physics of Plas-*
 439 *mas*, *22*(1), 12309. doi: 10.1063/1.4906356
- 440 Huang, S. Y., Sahraoui, F., Yuan, Z. G., He, J. S., Zhao, J. S., Contel, O. L., . . .
 441 Burch, J. L. (2017). Magnetospheric Multiscale Observations of Electron Vor-
 442 tex Magnetic Hole in the Turbulent Magnetosheath Plasma. *The Astrophysical*
 443 *Journal*, *836*(2), L27. doi: 10.3847/2041-8213/aa5f50
- 444 Johnson, J. R., & Cheng, C. Z. (1997, 4). Global structure of mirror modes in the
 445 magnetosheath. *Journal of Geophysical Research (Space Physics)*, *102*, 7179–
 446 7190. doi: 10.1029/96JA03949
- 447 Kasper, J. C., Abiad, R., Austin, G., Balat-Pichelin, M., Bale, S. D., Belcher,
 448 J. W., . . . Zank, G. (2016, 12). Solar Wind Electrons Alphas and Protons
 449 (SWEAP) Investigation: Design of the Solar Wind and Coronal Plasma In-
 450 strument Suite for Solar Probe Plus. *Space Science Reviews*, *204*(1), 131–

- 451 186. Retrieved from <https://doi.org/10.1007/s11214-015-0206-3> doi:
452 10.1007/s11214-015-0206-3
- 453 Kuznetsov, E. A., Passot, T., & Sulem, P. L. (2008). Nonlinear theory of mirror
454 instability near its threshold. *JETP Letters*, *86*(10), 637–642. doi: 10.1134/
455 S0021364007220055
- 456 Liu, H., Zong, Q. G., Zhang, H., Xiao, C. J., Shi, Q. Q., Yao, S. T., ... Rankin,
457 R. (2019). MMS observations of electron scale magnetic cavity embedded
458 in proton scale magnetic cavity. *Nature Communications*, *10*(1), 1–11. doi:
459 10.1038/s41467-019-08971-y
- 460 Malaspina, D. M., Ergun, R. E., Bolton, M., Kien, M., Summers, D., Stevens, K., ...
461 Goetz, K. (2016). The Digital Fields Board for the FIELDS instrument suite
462 on the Solar Probe Plus mission: Analog and digital signal processing. *Journal*
463 *of Geophysical Research: Space Physics*. doi: 10.1002/2016JA022344
- 464 Roytershteyn, V., Karimabadi, H., & Roberts, A. (2015). Generation of magnetic
465 holes in fully kinetic simulations of collisionless turbulence. *Philosophical*
466 *Transactions of the Royal Society A: Mathematical, Physical and Engineering*
467 *Sciences*, *373*(2041), 1–13. doi: 10.1098/rsta.2014.0151
- 468 Russell, C. T., Jian, L. K., Luhmann, J. G., Zhang, T. L., Neubauer, F. M., Skoug,
469 R. M., ... Cowee, M. M. (2008, 8). Mirror mode waves: Messengers from
470 the coronal heating region. *Geophysical Research Letters*, *35*, L15101. doi:
471 10.1029/2008GL034096
- 472 Soucek, J., Lucek, E., & Dandouras, I. (2008, 4). Properties of magnetosheath
473 mirror modes observed by Cluster and their response to changes in plasma
474 parameters. *Journal of Geophysical Research (Space Physics)*, *113*, A04203.
475 doi: 10.1029/2007JA012649
- 476 Southwood, D. J., & Kivelson, M. G. (1993). Mirror instability: 1. Physical mecha-
477 nism of linear instability. *Journal of Geophysical Research*, *98*(A6), 9181. doi:
478 10.1029/92ja02837
- 479 Stix, T. H. (1992). *Waves in plasmas*. AIP-Press.
- 480 Sun, W. J., Shi, Q. Q., Fu, S. Y., Pu, Z. Y., Dunlop, M. W., Walsh, A. P.,
481 ... Fazakerley, A. (2012, 3). Cluster and TC-1 observation of mag-
482 netic holes in the plasma sheet. *Annales Geophysicae*, *30*, 583–595. doi:
483 10.5194/angeo-30-583-2012

- 484 Sundberg, T., Burgess, D., & Haynes, C. T. (2015, 4). Properties and ori-
 485 gin of subproton-scale magnetic holes in the terrestrial plasma sheet.
 486 *Journal of Geophysical Research (Space Physics)*, *120*, 2600–2615. doi:
 487 10.1002/2014JA020856
- 488 Tenerani, A., Califano, F., Pegoraro, F., & Le Contel, O. (2012, 5). Coupling be-
 489 tween whistler waves and slow-mode solitary waves. *Physics of Plasmas*, *19*(5),
 490 52103. doi: 10.1063/1.4717764
- 491 Tenerani, A., Contel, O. L., Califano, F., Robert, P., Fontaine, D., Cornilleau-
 492 Wehrlin, N., & Sauvaud, J.-A. (2013, 10). Cluster observations of whistler
 493 waves correlated with ion-scale magnetic structures during the 17 August
 494 2003 substorm event. *Journal of Geophysical Research (Space Physics)*, *118*,
 495 6072–6089. doi: 10.1002/jgra.50562
- 496 Whittlesey, P. L., Larson, D. E., Kasper, J. C., Halekas, J., Abatcha, M., Abiad,
 497 R., . . . Verniero, J. L. (2020). The Solar Probe ANalyzersElectrons on the
 498 Parker Solar Probe. *The Astrophysical Journal Supplement Series*, *246*(2),
 499 74. Retrieved from <http://dx.doi.org/10.3847/1538-4365/ab7370> doi:
 500 10.3847/1538-4365/ab7370
- 501 Wintertialter, D., Neugebauer, M., Goldstein, B. E., Smith, E. J., Bame, S. J., &
 502 Balogh, A. (1994). Ulysses field and plasma observations of magnetic holes
 503 in the solar wind and their relation to mirror-mode structures. *Journal of*
 504 *Geophysical Research: Space Physics*. doi: 10.1029/94JA01977
- 505 Yao, S. T., Wang, X. G., Shi, Q. Q., Pitkänen, T., Hamrin, M., Yao, Z. H., . . . Liu,
 506 J. (2017). Observations of kinetic-size magnetic holes in the magnetosheath.
 507 *Journal of Geophysical Research: Space Physics*, *122*(2), 1990–2000. doi:
 508 10.1002/2016JA023858

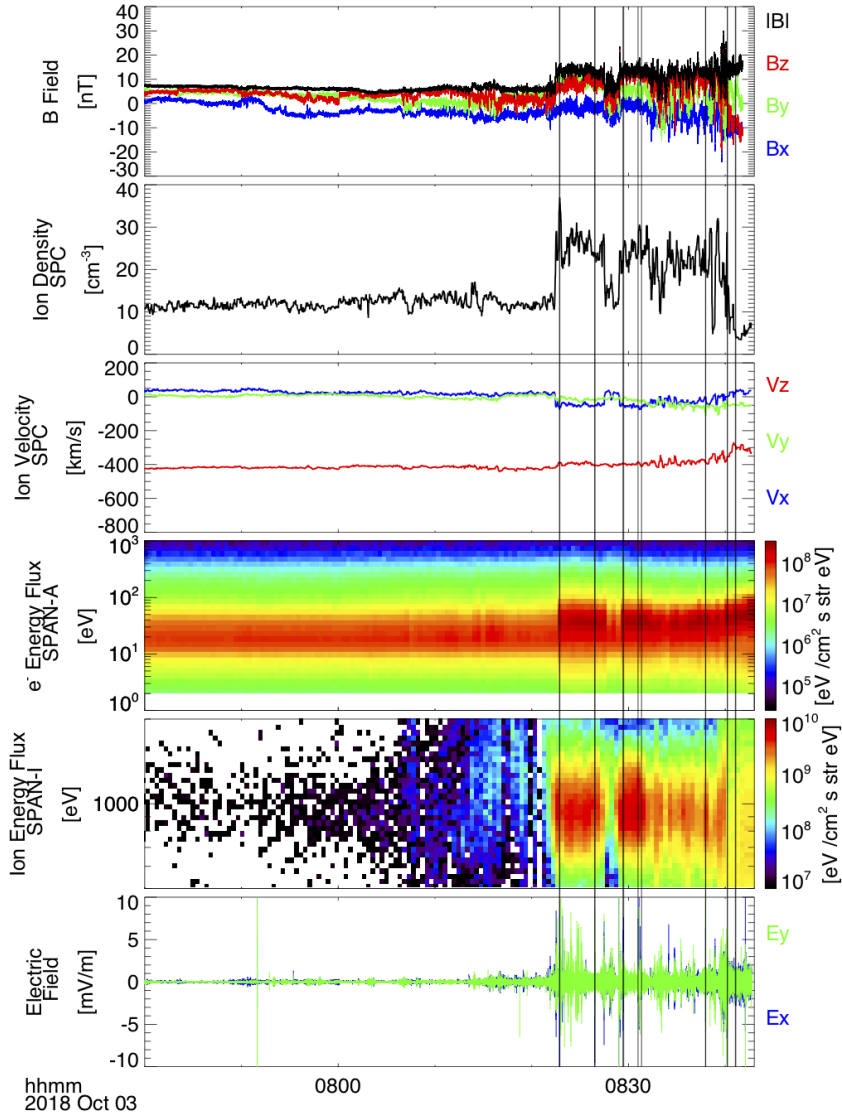


Figure 1. Overview of the first Venus Flyby undertaken by Parker Solar Probe. The plot shows, in descending order, magnetic field, proton density from SPC, proton velocity from SPC, electron energy flux, proton energy flux from SPAN-ion, and electric field. All vectors are in spacecraft coordinates. The Parker spacecraft initially measured solar wind before encountering the Venusian shock at $\sim 08:22:20$ UTC. It then observed the Venusian magnetosheath as well as other bow shock crossings before the end of the encounter at $\sim 08:50$. All vertical lines mark times in which sub-proton-scale magnetic holes were observed.

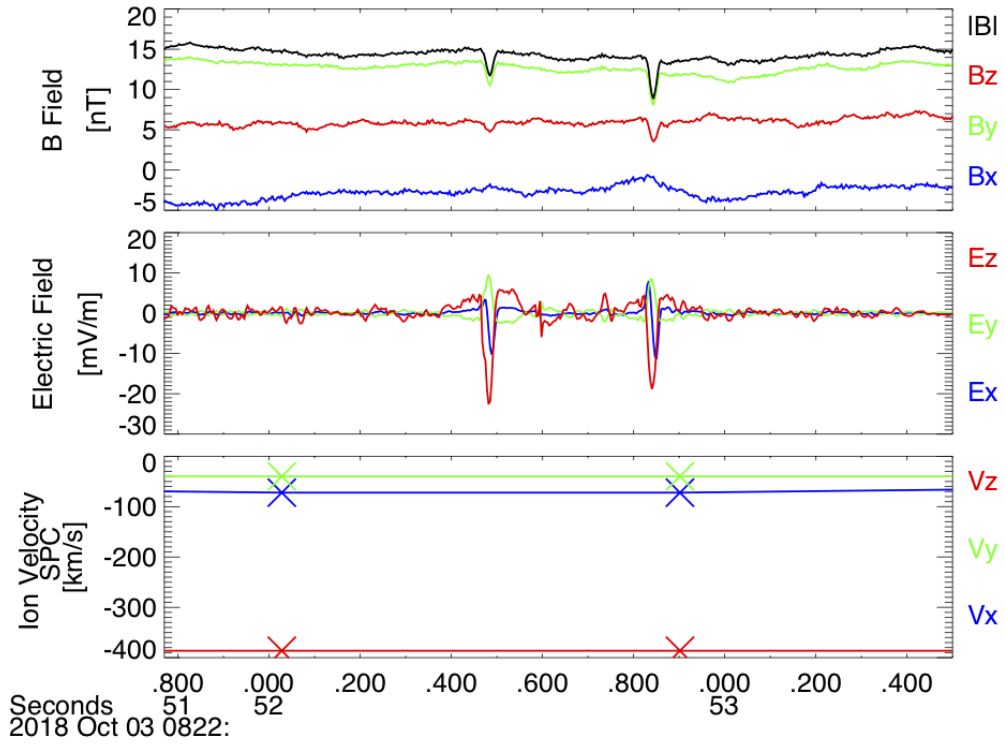


Figure 2. Two example magnetic hole candidates. This figure shows a 1.6 second zoomed in view of the magnetic field, electric field, and proton velocity at \sim 08:22:52 UTC, approximately 30 seconds after Parker Solar Probe made its initial Venusian bow shock crossing. Bipolar and unipolar electric field signatures are observed in tandem with localized (50 ms) depressions in magnetic field strength.

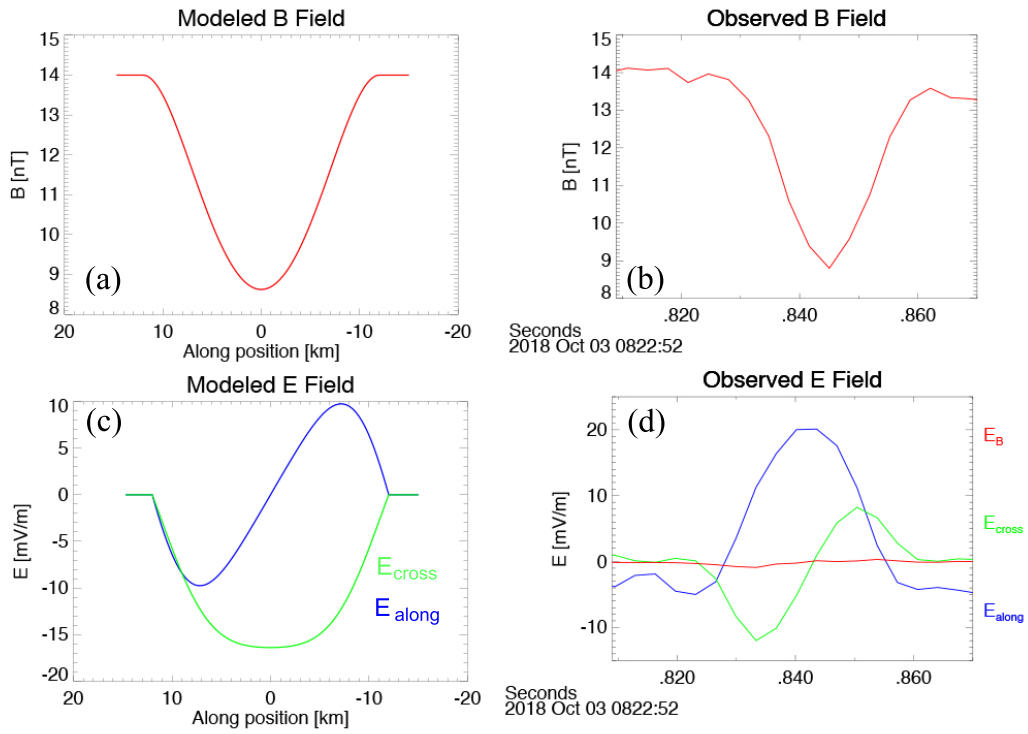


Figure 3. This figure shows a direct comparison between magnetic (a) and electric (c) field from the modeled electron vortex and the magnetic (b) and electric (d) field observed by Parker in the Venusian magnetosheath. The observed magnetic and electric field were transformed into the local plasma frame.

Figure 1.

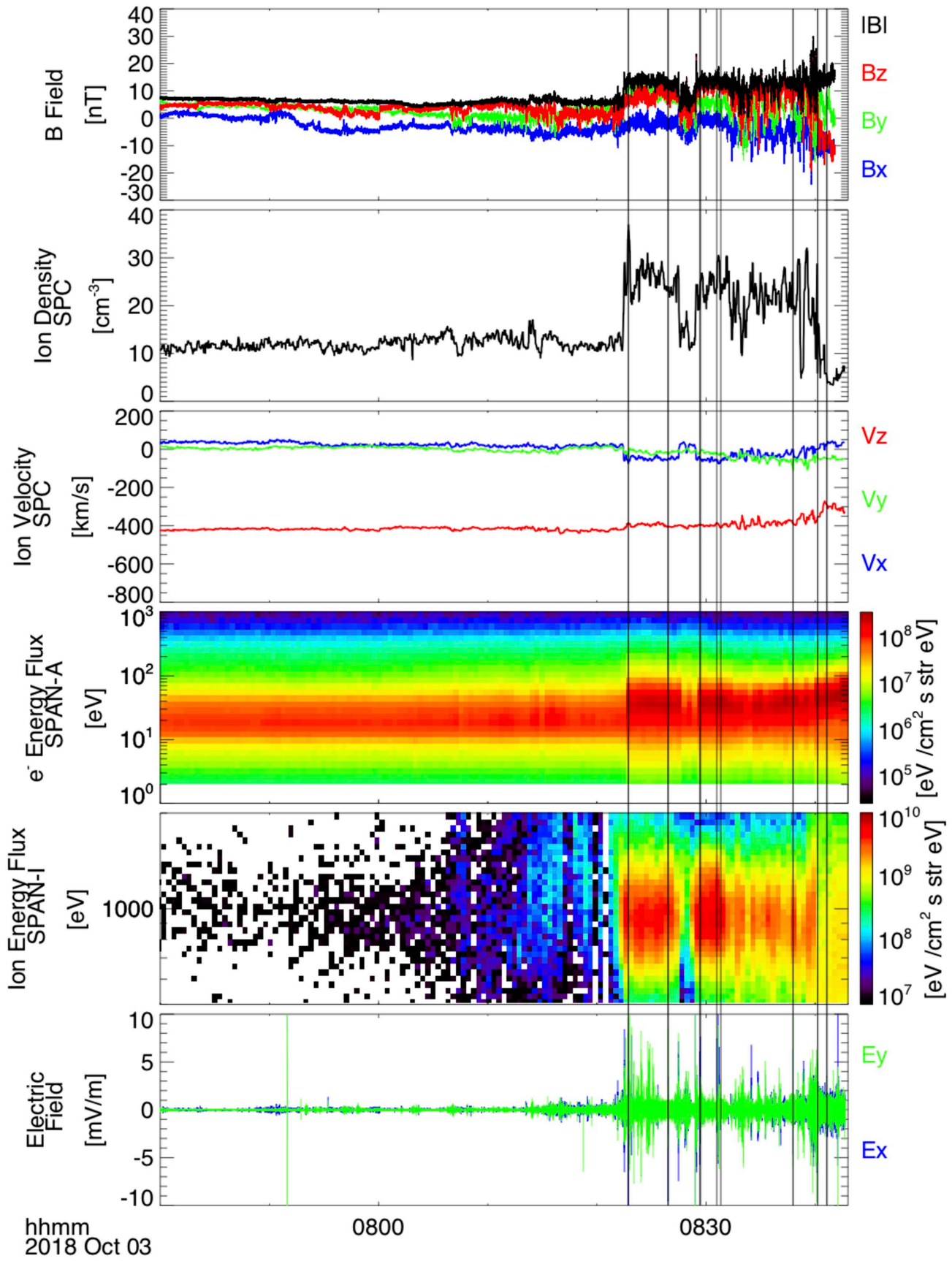


Figure 2.

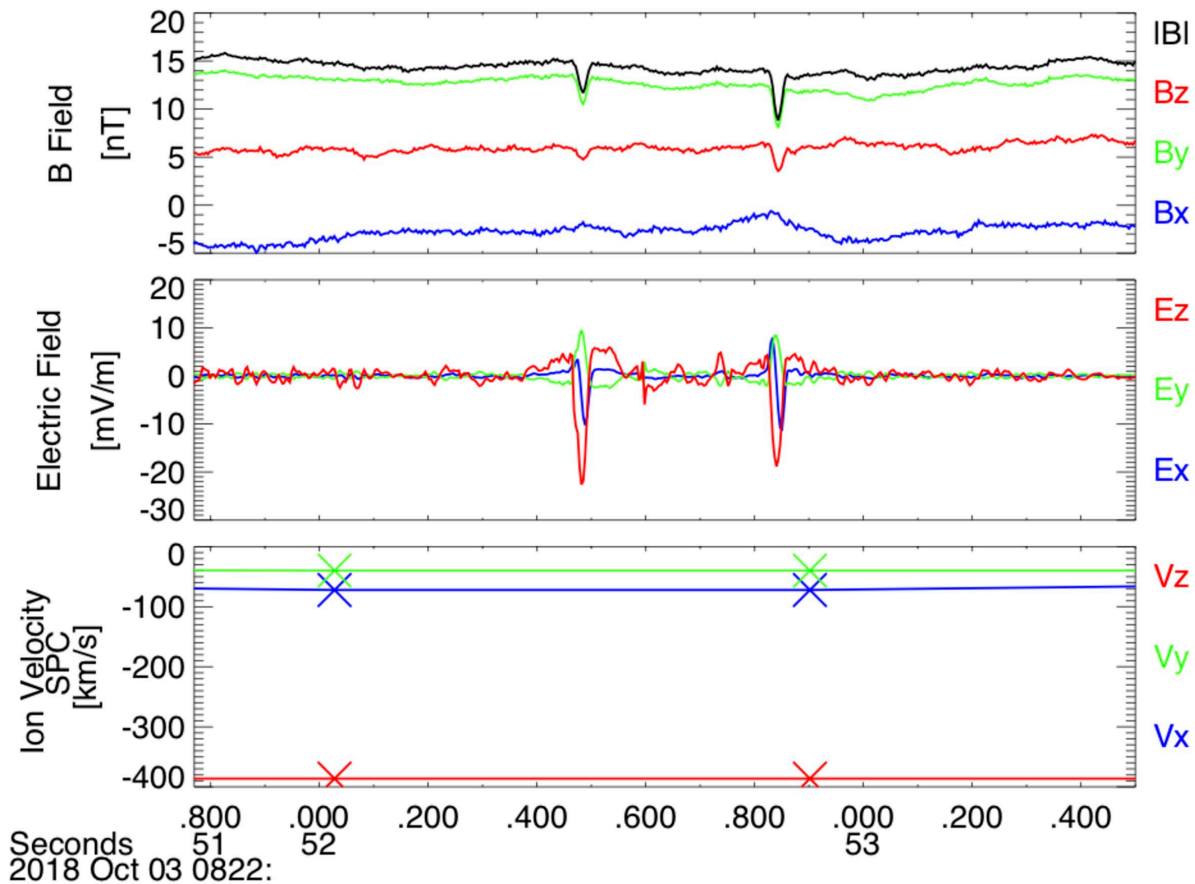
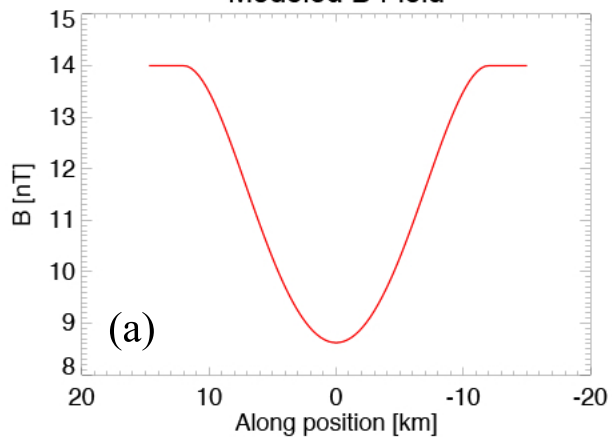
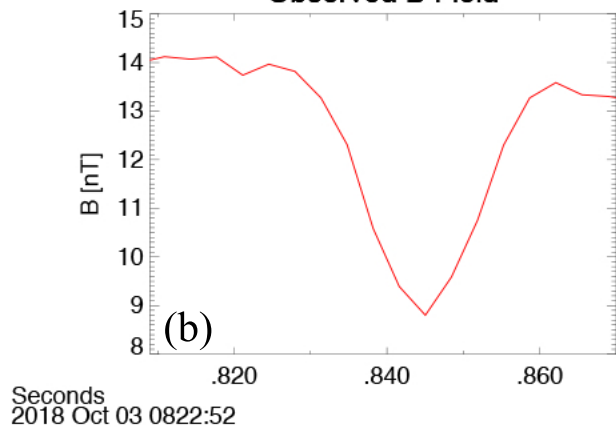


Figure 3.

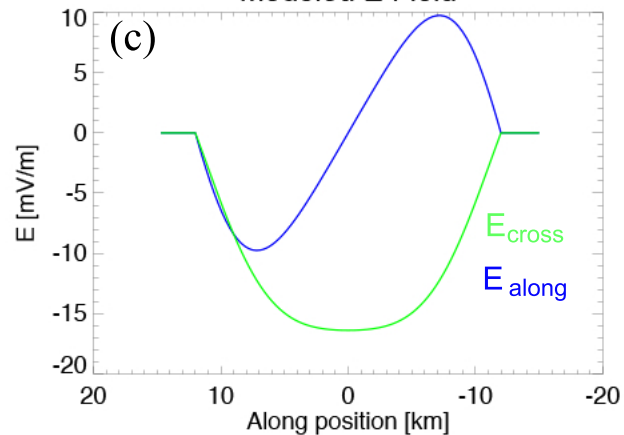
Modeled B Field



Observed B Field



Modeled E Field



Observed E Field

